INTERNATIONAL JOURNAL FOR NUMERICAL METHODS IN FLUIDS
Int. J. Numer. Meth. Fluids 2004; **44**:505–523 (DOI: 10.1002/fld.652)

Higher-order upwind leapfrog methods for multi-dimensional acoustic equations

Cheolwan Kim*,†,‡

Aerodynamics Department, Korea Aerospace Research Institute, 45 Eoeun-Dong, Youseong-Gu, Daejeon, 305-333, South Korea

SUMMARY

A non-dissipative and very accurate one-dimensional upwind leapfrog method was successfully extended to higher-order and multi-dimensional acoustic equations. The governing equations in characteristic form and staggered grid were utilized to preserve the accuracy. Fourier analysis was performed to find the accurate scheme for acoustics and the resultant two-dimensional methods were successfully applied to several classical test cases. Copyright © 2004 John Wiley & Sons, Ltd.

KEY WORDS: acoustic waves; upwind leapfrog scheme; non-square grid

1. INTRODUCTION

Sound propagation is represented by the unsteady linearized Euler equations and characterized as long-range propagation of high-frequency waves, so that all numerical schemes to simulate the sound propagation would have very low dissipation and few dispersion errors. Otherwise, acoustic wave will be dissipated mostly and located in the wrong place after traveling over several wavelengths.

Recently, several higher-order numerical schemes have been developed for precise evaluation of acoustic wave [1] and one of them is the upwind leapfrog scheme, whose one-dimensional advection version was proposed by Iserles [2]. Compared to the regular leapfrog method, the upwind leapfrog scheme is more compact and accurate because it is combined with upwind bias. Roe *et al.* [3] further investigated the upwind leapfrog scheme to evaluate the applicability of this method to linear high-frequency wave propagation problems in acoustics/aeroacoustics, electromagnetics and elastodynamics, etc. Roe and Thomas [4] developed the fourth-order scheme by extending the stencil in space and time domain as well

*Correspondence to: Cheolwan Kim, Aerodynamics Department, Korea Aerospace Research Institute, 45 Eoeun-Dong, Youseong-Gu, 305-333 Daejeon, South Korea.
† E-mail: cwkim@kari.re.kr
‡ Senior Researcher.

Received 16 September 2002
Revised 5 August 2003

as multi-dimensional second-order scheme for linear wave system, especially for acoustics by using the bicharacteristic theory. They devised the staggered grid technique storing values at the cell edge not to introduce any numerical dissipation error [5]. Meanwhile, Nguyen and Roe compared phase properties of multi-dimensional upwind leapfrog method and Yee's standard leapfrog method for acoustics and electromagnetics [6]. Thomas, then developed a fourth-order version of the upwind leapfrog method for acoustic wave simulation but its application is limited because of its stability problem. In this paper, this limitation is resolved and a higher-order scheme, stable even on non-square grid, is extended to the system of equations expressed in polar co-ordinates.

The development of multi-dimensional upwind leapfrog schemes for acoustics and staggered grid strategy are explained in Section 2. In Section 3, a higher-order upwind leapfrog scheme for acoustics is demonstrated with a solution to its stability problems. The higher-order scheme described here is stable on even non-square Cartesian grid and it can be applied to acoustics in polar co-ordinates. The second- and fourth-order upwind leapfrog schemes are tested for well-known test cases.

2. MULTI-DIMENSIONAL ACOUSTICS

Multi-dimensional acoustics is also represented by the linearized Euler equations. The equations having pressure and velocity fluctuations ($p, \mathbf{u} = [u, v, w]$) are

$$\begin{aligned} \frac{\partial p}{\partial t} + \rho_0 a_0^2 \nabla \cdot \mathbf{u} &= 0 \\ \frac{\partial \mathbf{u}}{\partial t} + \frac{1}{\rho_0} \nabla p &= 0 \end{aligned} \tag{1}$$

where ρ_0 and a_0 are steady state values of density and speed of sound.

2.1. Characteristic form of equations

To develop the upwind leapfrog method for acoustics, the system of Equations (1) is arranged in characteristic form which is quite similar to the advection equation, because characteristic form of equation clarifies wave propagation direction. A system of equations in N-dimensional space can be written in vector form as follows.

$$\mathbf{U}_t + \sum_{1 \leqslant d \leqslant N} \mathbf{A}_d \cdot \frac{\partial \mathbf{U}}{\partial \mathbf{x}_d} = 0 \tag{2}$$

To study wave propagation in the direction $\mathbf{x}_1$, this equation was multiplied by l_1, a left eigenvector of $\mathbf{A}_1$ having eigenvalue λ_1. This multiplication rotates the co-ordinate to be aligned with the arbitrary direction of interest, $\mathbf{x}_1$. The result, called a characteristic equation, is

$$\left(\frac{\partial}{\partial t} + \lambda_1 \frac{\partial}{\partial \mathbf{x}_1} \right) (l_1 \mathbf{U}) + \sum_{2 \leqslant d \leqslant N} l_1 \mathbf{A}_d \frac{\partial \mathbf{U}}{\partial \mathbf{x}_d} = 0 \tag{3}$$

In two-dimensional acoustics, the variables $\mathbf{x}$, $\mathbf{U}$ and the constant matrices $\mathbf{A}_1$ and $\mathbf{A}_2$ are

$$\mathbf{x}=\begin{bmatrix} x \\ y \end{bmatrix}, \quad \mathbf{U}=\begin{bmatrix} p \\ u \\ v \end{bmatrix}, \quad \mathbf{A}_1=\begin{bmatrix} 0 & \rho_0 a_0^2 & 0 \\ 1/\rho_0 & 0 & 0 \\ 0 & 0 & 0 \end{bmatrix}, \quad \mathbf{A}_2=\begin{bmatrix} 0 & 0 & \rho_0 a_0^2 \\ 0 & 0 & 0 \\ 1/\rho_0 & 0 & 0 \end{bmatrix}$$

The eigenvalues of $\mathbf{A}_1$ are $\lambda=\pm a_0, 0$. The eigenvector corresponding to $\lambda=0$ does not produce any interesting result, but the remaining other eigenvectors, $(1, \pm \rho_0 a_0, 0)$ yield the following characteristic equations.

$$\frac{\partial}{\partial t}(p \pm \rho_0 a_0 u) \pm a_0 \frac{\partial}{\partial x}(p \pm \rho_0 a_0 u) = -\rho_0 a_0^2 v_y \tag{4}$$

These are the characteristic equations for plane waves traveling in the $\pm x$-directions. The characteristic equations for waves traveling in the $\pm y$-directions are

$$\frac{\partial}{\partial t}(p \pm \rho_0 a_0 v) \pm a_0 \frac{\partial}{\partial y}(p \pm \rho_0 a_0 v) = -\rho_0 a_0^2 u_x \tag{5}$$

For a wave moving in arbitrary direction, the characteristic equation is generated by multiplying the system (2) by $\mathbf{l}=(1, \rho_0 a_0 \cos\theta, \rho_0 a_0 \sin\theta)$.

$$\begin{aligned} &\left(\frac{\partial}{\partial t}+a_0\cos\theta\frac{\partial}{\partial x}+a_0\sin\theta\frac{\partial}{\partial y}\right)[p+\rho_0 a_0(u\cos\theta+v\sin\theta)] \\ &\quad = -\rho_0 a_0^2\left[\left(\sin\theta\frac{\partial}{\partial x}-\cos\theta\frac{\partial}{\partial y}\right)(u\cos\theta-v\sin\theta)\right] \end{aligned} \tag{6}$$

When $\theta=0$ or π, the above equation is simplified to Equation (4). For any direction θ, the left-hand side of the above characteristic equation (6) is a one-dimensional characteristic equation along a generator of the Mach cone

$$\mathrm{d}x^2+\mathrm{d}y^2=a_0^2\,\mathrm{d}t^2$$

and the right-hand side is the derivative tangential to the cone. Figure 1 shows the Mach cone and the characteristic plane for the wave moving in the positive x-direction.

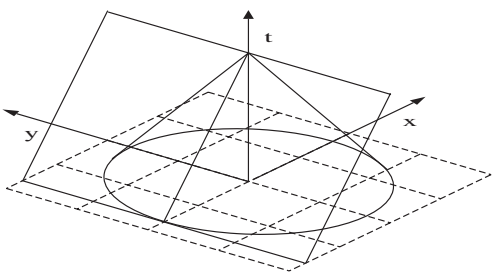

Figure 1. Characteristic planes for wave moving in the positive x-direction.

2.2. Second-order upwind leapfrog scheme

Characteristic equations aligned along x- and y-axis are used as the governing equations of two-dimensional acoustics and expressed as follows.

$$\frac{\partial}{\partial t}(p \pm \rho_0 a_0 u) \pm a_0 \frac{\partial}{\partial x}(p \pm \rho_0 a_0 u) = -\rho_0 a_0^2 \frac{\partial v}{\partial y} \tag{7}$$

These are the characteristic equations for plane waves traveling in the $\pm x$-directions. The characteristic equations for waves traveling in the $\pm y$-directions are

$$\frac{\partial}{\partial t}(p \pm \rho_0 a_0 v) \pm a_0 \frac{\partial}{\partial y}(p \pm \rho_0 a_0 v) = -\rho_0 a_0^2 \frac{\partial u}{\partial x} \tag{8}$$

Since the left-hand sides of the above equations resemble one-dimensional advection equation, they can be discretized in the same way as the one-dimensional scheme. The right-hand sides are discretized by central differencing. As a typical difficulty encountered in application of characteristic equations, three unknown variables should be updated in two-dimensional acoustics although the characteristic method provides four relations and the pressure is updated twice. Two pressures are identical analytically but may be different in numerical computation. Two methods are presented in this section for the discretization of the characteristic methods. For convenience the variables p, u, v are non-dimensionalized and steady values of density and speed of sound ρ_0, a_0 are set to unity.

The first method is to discretize the equations on uniform grid which stores every solution at cell node. The characteristic equation aligned in the positive x-direction is discretized as following Equation (9) on the stencil as illustrated in Figure 2(a).

$$\delta_t(p+u)^{n+1/2}_{j,k} + \delta_t(p+u)^{n-1/2}_{j-1,k} + 2\nu_x \delta_x (p+u)^n_{j-1/2,k} + 2\nu_y \mu_x \mu_y \delta_y v_{j-1/2,k} = 0 \tag{9}$$

where $\nu_x = \Delta t/\Delta x$, $\nu_y = \Delta t/\Delta y$. Also the differencing and averaging operators are

$$\delta_t w^n_{j,k} = w^{n+1/2}_{j,k} - w^{n-1/2}_{j,k}, \quad \mu_t w^n_{j,k} = \frac{1}{2}(w^{n+1/2}_{j,k} + w^{n-1/2}_{j,k})$$

$$\delta_x w^n_{j,k} = w^n_{j+1/2,k} - w^n_{j-1/2,k}, \quad \mu_x w^n_{j,k} = \frac{1}{2}(w^n_{j+1/2,k} + w^n_{j-1/2,k})$$

$$\delta_y w^n_{j,k} = w^n_{j,k+1/2} - w^n_{j,k-1/2}, \quad \mu_x w^n_{j,k} = \frac{1}{2}(w^n_{j,k+1/2} + w^n_{j,k-1/2})$$

Other characteristic equations are also discretized in the same way. For example, the finite difference equation for $(p-u)$ wave is

$$\delta_t(p-u)^{n+1/2}_{j,k} + \delta_t(p+u)^{n-1/2}_{j+1,k} - 2\nu_x \delta_x (p-u)^n_{j+1/2,k} + 2\nu_y \mu_x \mu_y \delta_y v_{j+12,k} = 0 \tag{10}$$

Equations (9) and (10) are used to update p and u. Two other equations not shown here are used to update p and v. Two pressures updated in different ways are not identical and averaged. This averaging, however destroys the time-reversibility of the overall scheme and introduces some dissipation.

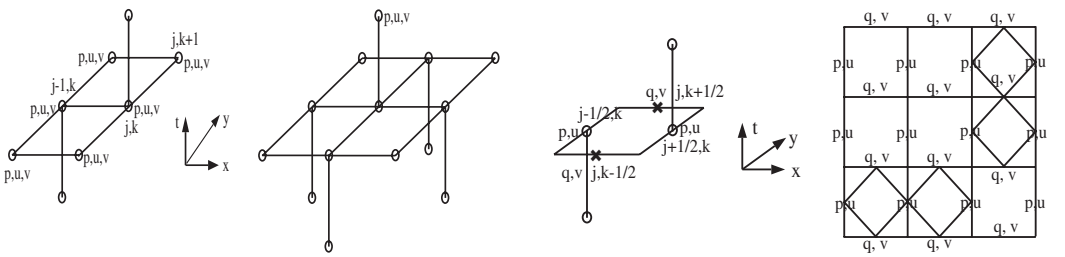

Figure 2. Stencils of second-order upwind leapfrog methods: (a) uniform grid; and (b) staggered grid.

The second method developed by Roe and Thomas [4], is to utilize the staggered grid storing the variables as shown in Figure 2(b). The pressure updated with u is stored with u and the other pressure with v is stored with v. The pressure updated with v is described as q for convenience. Therefore, the characteristic equations are

$$\frac{\partial}{\partial t}(p \pm u) \pm \frac{\partial}{\partial x}(p \pm u) = -\frac{\partial v}{\partial y} \tag{11}$$

$$\frac{\partial}{\partial t}(q \pm v) \pm \frac{\partial}{\partial x}(q \pm v) = -\frac{\partial u}{\partial x} \tag{12}$$

and discretized on the staggered grid, illustrated in Figure 2(b) as follows.

$$\begin{aligned}
\delta_t(p+u)^{n+1/2}_{j+1/2,k} + \delta_t(p+u)^{n-1/2}_{j-1/2,k} + 2v_x\delta_x(p+u)^n_{j,k} + 2v_y\delta_y v_{j,k} &= 0 \\
\delta_t(p-u)^{n+1/2}_{j-1/2,k} + \delta_t(p-u)^{n-1/2}_{j+1/2,k} - 2v_x\delta_x(p-u)^n_{j,k} + 2v_y\delta_y v_{j,k} &= 0 \\
\delta_t(q+v)^{n+1/2}_{j,k+1/2} + \delta_t(q+v)^{n-1/2}_{j,k-1/2} + 2v_y\delta_y(q+v)^n_{j,k} + 2v_x\delta_x u_{j,k} &= 0 \\
\delta_t(q-v)^{n+1/2}_{j,k-1/2} + \delta_t(q-v)^{n-1/2}_{j,k+1/2} - 2v_y\delta_y(q-v)^n_{j,k} + 2v_x\delta_x u_{j,k} &= 0
\end{aligned} \tag{13}$$

This method eliminated the averaging of pressures and updated the solutions without any dissipation. Furthermore, the staggered grid provides a compact stencil, which is considered as another advantages of the staggered grid compared to the uniform grid.

2.3. Error analysis

For error analysis, solutions are assumed to have the form

$$\begin{bmatrix} p \\ u \\ v \end{bmatrix}(x,y,t) = \begin{bmatrix} P \\ U \\ V \end{bmatrix} \exp[\mathrm{i}(\omega t - k_x x - k_y y)] = \begin{bmatrix} P \\ U \\ V \end{bmatrix} \exp\left[\mathrm{i}\left(\frac{\phi t}{\Delta t} - \frac{\theta_x x}{\Delta x} - \frac{\theta_y y}{\Delta y}\right)\right] \tag{14}$$

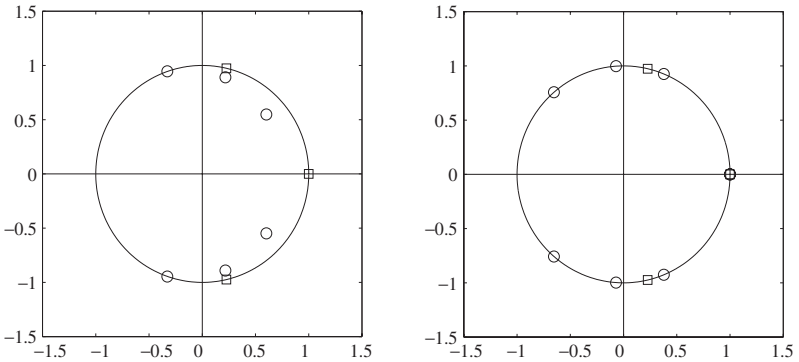

Figure 3. Eigenmodes of second-order upwind leapfrog method, $v_x = \frac{1}{4}$, $v_y = \frac{1}{2}$, $\theta_x = 3\pi/5$, $\theta_y = 4\pi/5$. (a) Uniform grid, (b) Staggered grid.

where $\phi = \omega \cdot \Delta t$, $\theta_x = k_x \cdot \Delta x$, $\theta_y = k_y \cdot \Delta y$ and $[P, U, V]^{\mathrm{T}}$ are magnitudes of $[p, u, v]^{\mathrm{T}}$. Substituting the above relations into Equations (1) yields the exact phase speed ϕ_e as

$$\phi_e = \begin{pmatrix} 0 \\ \pm\sqrt{v_x^2\theta_x^2 + v_y^2\theta_y^2} \end{pmatrix} \tag{15}$$

The first solution, $\phi_e = 0$ represents vorticity mode. The second and third ones represent the exact phase speeds of acoustic modes moving forward and backward.

To investigate the structure of eigenmodes, the amplification factors, $\exp(\mathrm{i}\phi)$ are drawn on complex domain for given Courant numbers and Fourier angles because ϕ is a complex number ($\phi = \phi_r + \mathrm{i}\phi_i$). Figure 3 shows the eigenmodes when $v_x = \frac{1}{4}$, $v_y = \frac{1}{2}$, $\theta_x = 3\pi/5$ and $\theta_y = 4\pi/5$. The square and circle symbols represent the analytic and numerical eigenmodes, respectively. An eigenmode lying on the unit circle indicates that its amplification factor is unity and it is updated without dissipation. The abscissa and ordinate of Figure 3 are the real and imaginary part of $\exp(\mathrm{i}\phi)$ respectively. Figure 3(a) shows the eigenmodes of the second-order scheme on a uniform grid. Some modes lying inside unit circle show that averaging two pressures updated by different schemes does indeed introduce dissipation. Every eigenmode of the staggered grid, however lies on the unit circle, Figure 3(b) and updates the solution without any dissipation. To investigate properties of the scheme, we focus on the forward-moving acoustic wave whose exact phase should be $\phi_e = \sqrt{v_x^2\theta_x^2 + v_y^2\theta_y^2}$. The dissipation and dispersion errors are defined as

$$D(\%) = [1 - (\exp(-\phi_i))^{N/v}] \times 100, \tag{16}$$

$$E(\%) = \left(\frac{\phi_r}{\phi_e (= v_x\theta_x + v_y\theta_y)} - 1 \right) \times 100 \tag{17}$$

Courant numbers are $v_x = v_y = \frac{1}{3}$ and the wave front direction which is defined as $\tan^{-1}(k_y/k_x)$ and denoted by α, is varied from the positive x-axis to the positive y-axis. Therefore the

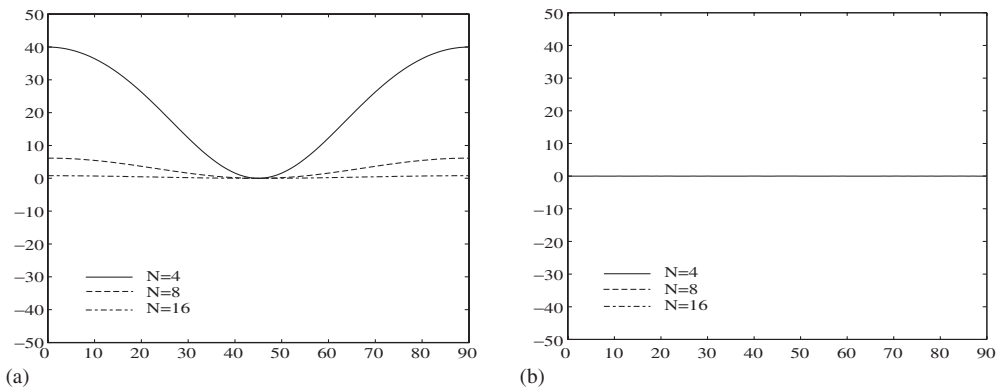

Figure 4. Dissipation errors of three-level second-order upwind leapfrog method. $v_x = v_y = 1/3$. (a) Uniform grid, (b) Staggered grid.

Fourier angles θ_x and θ_y, cells-per-wavelength N and wave front angle α have the following relations.

$$\theta_x = \frac{2\pi}{N}\cos\alpha, \qquad \theta_y = \frac{2\pi}{N}\sin\alpha \tag{18}$$

Numbers 4, 8 and 16 are chosen for N to clarify the accuracy trend. Figure 4 shows the dissipation errors of the uniform and staggered grid. As confirmed from the eigenmode plot, Figure 4(a) the uniform grid scheme is dissipative and shows the highest dissipation when the wave front direction is parallel to the coordinates. Averaging two pressure modes may behave like a blending function. However, the staggered grid technique does not show any dissipation error, Figure 4(b).

Compared with the uniform grid, the staggered grid technique has some nice properties justifying further development of the upwind leapfrog scheme for multi-dimensional acoustics. They are (1) improving resolution, (2) making the stencil compact and (3) having no dissipation error.

2.4. Higher-order upwind leapfrog methods

To develop higher-order scheme, the stencil of the second-order scheme, Figure 2(b) was extended in either time or space as done in one-dimension. Extending in time domain provides some degrees of freedom which cancel out the second-order truncation error terms of the modified equation. However the additional degrees of freedom are not sufficient to eliminate every error term and the resultant scheme is still second-order although this extension improves the resolution.

The stencil for the wave moving in the positive x-axis is shown in Figure 5(a) and the difference equation is

$$\begin{aligned} &c_1[\delta_t(p+u)^{n+1}_{j+1/2,k} + \delta_t(p+u)^{n-1}_{j-1/2,k}] + c_2[\delta_t(p+u)^{n}_{j+1/2,k} + \delta_t(p+u)^{n}_{j-1/2,k}] \\ &\quad + v_x\mu_t\delta_x(p+u)^n_{j,k} + v_y\mu_t\delta_y v^n_{j,k} = 0 \end{aligned} \tag{19}$$

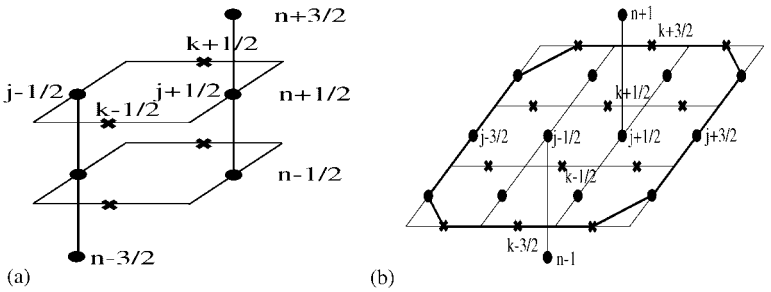

Figure 5. Stencils of higher-order upwind leapfrog schemes for the wave moving in positive x-axis: (a) four-level second-order compact stencil; and (b) three-level fourth-order space-extended stencil.

where $c_1 = (v_x + 1)/6v_x$, $c_2 = (5v_x - 1)/6v_x$ and they are determined by eliminating a second-order error term, $\partial^3 p/\partial x^3$.

Other characteristic equations can be discretized in a similar way. The remaining second-order error terms of the above scheme (19) is

$$-\frac{\Delta t^2}{24}\left(\frac{2}{v_x}\frac{\partial^3 q}{\partial x \partial y^2} - \frac{2}{v_x}\frac{\partial^3 u}{\partial x \partial y^2} - \frac{1}{v_x^2}\frac{\partial^3 v}{\partial x^2 \partial y} + \frac{v_x - 2v_y^2}{v_x v_y^2}\frac{\partial^3 v}{\partial y^3}\right) \tag{20}$$

and these terms are derived by replacing the time-derivative terms with the space-derivative terms. The governing equations provide the relations of even higher-order derivative terms(Lax-Wendroff type derivation). More degrees of freedom are required to discretize these terms. Additional extension in time however, does not achieve the fourth-order accuracy and it is not considered here.

Although extending the second-order stencil in space sacrifices the comapctness, it is currently the only way to increase the order of accuracy up to four that we have found. This scheme has difficulty in applying at computational boundaries but its excellent phase property makes the use of this scheme for the interior points very attractive. Developing a three-level fourth-order scheme would be straightforward if stability were not an issue. The second-order scheme for $(p + u)$ wave with the second-order error terms is

$$\begin{aligned}
&\delta_t(p+u)^{n+1/2}_{j+1/2,k} + \delta_t(p+u)^{n-1/2}_{j+1/2,k} + 2\delta_x(p+u)^n_{j,k} + 2\delta_y v^n_{j,k} \\
&\quad = -c_{p_{xxx}}\Delta x^3\frac{\partial^3 p}{\partial x^3} - c_{q_{xyy}}\Delta x\Delta y^2\frac{\partial^3 q}{\partial x \partial y^2} - c_{u_{xxx}}\Delta x^3\frac{\partial^3 u}{\partial x^3} \\
&\qquad - c_{u_{xyy}}\Delta x\Delta y^2\frac{\partial^3 u}{\partial x \partial y^2} - c_{v_{xxy}}\Delta x^2\Delta y\frac{\partial^3 v}{\partial x^2 \partial y} - c_{v_{yyy}}\Delta y^3\frac{\partial^3 v}{\partial y^3}
\end{aligned} \tag{21}$$

where

$$c_{p_{xxx}} = \frac{1}{6}(2v_x^3 - 3v_x^2 + v_x), \quad c_{q_{xyy}} = \frac{2}{3}v_y^2(2v_x - 3)$$

$$c_{u_{xxx}} = \frac{1}{6}(2v_x^3 - 3v_x^2 + v_x), \quad c_{u_{xyy}} = \frac{1}{3}v_x v_y^2$$

$$c_{v_{xxy}} = \frac{1}{12}v_y(4v_x^2 - 6v_x + 3), \quad c_{v_{yyy}} = \frac{1}{12}v_y(4v_y^2 - 1)$$

Then discretizing the second-order errors and moving them to the left-hand side increase the order of accuracy. The discretization is not unique and Thomas [8] suggested the following choices.

$$\Delta x^3 \frac{\partial^3 p}{\partial x^3} = \delta_x^3 p_{j,k}^n, \quad \Delta x^3 \frac{\partial^3 u}{\partial x^3} = \delta_x^3 u_{j,k}^n, \quad \Delta x \Delta y^2 \frac{\partial^3 u}{\partial x \partial y^2} = \delta_x \delta_y^2 u_{j,k}^n$$

$$\Delta x \Delta y^2 \frac{\partial^3 q}{\partial x \partial y^2} = \mu_x \mu_y \delta_x \delta_y^2 q_{j,k}^n, \quad \Delta x^2 \Delta y \frac{\partial^3 v}{\partial x^2 \partial y} = \delta_x^2 \delta_y \delta_y^2 v_{j,k}^n, \quad \Delta y^3 \frac{\partial^3 v}{\partial y^3} = \delta_y^3 v_{j,k}^n \tag{22}$$

It was revealed during the test of this scheme, however, that it was unstable on a non-square grid, i.e. $\Delta x \neq \Delta y$. Figure 6(a) shows the eigenmodes of that case. Two eigenmodes on the real axis are stationary and the product of their amplification factors is always one, say $|g_1| \cdot |g_2| = 1$. The mode marked outside the unit circle amplifies the mode excited by even round off error and makes it overwhelm the physical solution. Typically, a region of local instability occurs whose amplitude grows rapidly while others are remaining quite locally in space. A smoothing operator was devised to resolve the instability problem. An ideal smoothing operator should be one that attacks only the spurious modes, leaving the physical modes unchanged. Since observations showed the errors to be associated with vorticity, we

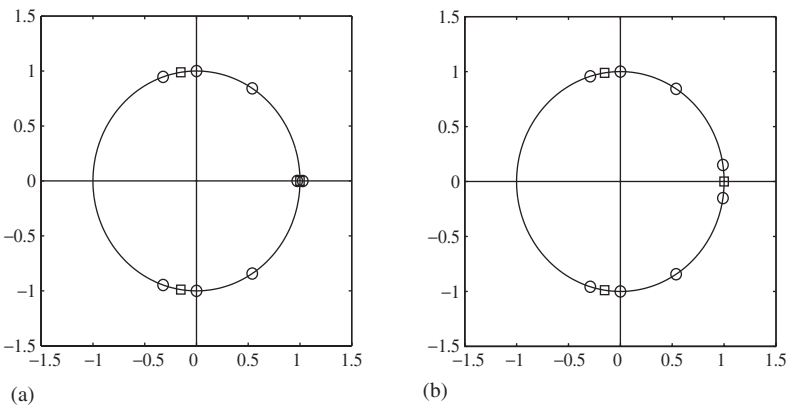

Figure 6. Eigenmodes of fourth-order upwind leapfrog methods: (a) original discretization; and (b) corrected discretization for second-order truncation error terms. $v_x = 1/4,\ v_y = 1/2,\ \theta_x = 9\pi/10,\ \theta_y = \pi.$

attempted a damping based on

$$\frac{\partial \mathbf{u}}{\partial t} = \varepsilon \cdot \nabla \times \mathbf{w} \tag{23}$$

where **u** is velocity vector and **w** is vorticity. Since **w** should vanish within truncation error, this smoothing operator leaves the order of accuracy unchanged, but it does not resolve the instability.

As an alternative, other choices of discretization for truncation error terms were examined and they turned out to resolve the instability. They are

$$\Delta x \Delta y^2 \frac{\partial^3 u}{\partial x \partial y^2} = \frac{1}{24}(28\delta_x \delta_y^2 - 4\mu_x^2 \delta_x \delta_y^2) u_{j,k}^n \tag{24}$$

$$\Delta x^2 \Delta y \frac{\partial^3 v}{\partial x^2 \partial y} = \frac{1}{24}(28\delta_x^2 \delta_y - 4\mu_y^2 \delta_x^2 \delta_y) v_{j,k}^n \tag{25}$$

Now every eigenmode, Figure 6(b) lies on the unit circle and the fourth-order scheme with corrected discretization is neutrally stable on non-square grid. However, it is very difficult to explain the role of new discretizations. It is worth observing, however, that the new discretization (24) involves data of points $(j \pm 3/2, k, k \pm 1)$ that are not used in (22).

Figure 7 compares the dispersion errors of three-level second-order, four-level second-order and three-level fourth-order upwind leapfrog schemes. Four-level second-order scheme shows a better resolution than three-level second-order scheme and the three-level fourth-order scheme has the best phase property.

2.5. *Accuracy comparison of leapfrog schemes*

Another leapfrog type scheme is Yee's standard leapfrog scheme, mainly designed for electromagnetics and acoustics. It stores pressure and velocities at cell centre and edges, respectively. Its accuracy is comparable to the upwind leapfrog method. Nguyen [6] compared phase properties of these schemes and concluded that floating point operations per cell of two-dimensional

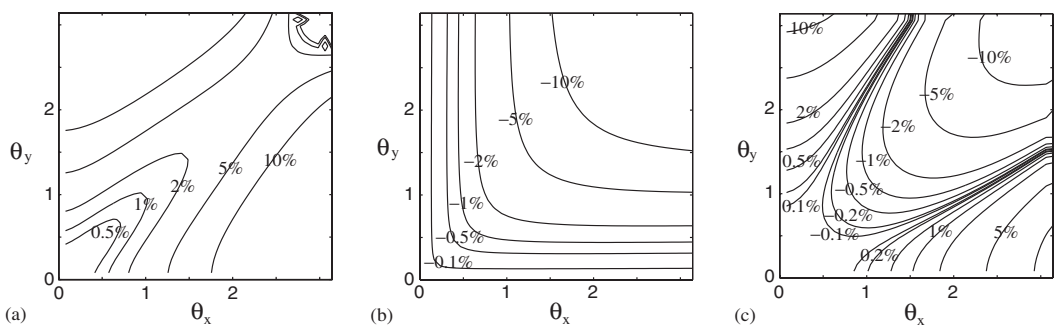

Figure 7. Dispersion errors of second- and fourth-order upwind leapfrog methods. Courant numbers, $v_x = v_y = 1/4$: (a) three-level second-order; (b) four-level second-order; and (c) three-level fourth-order.

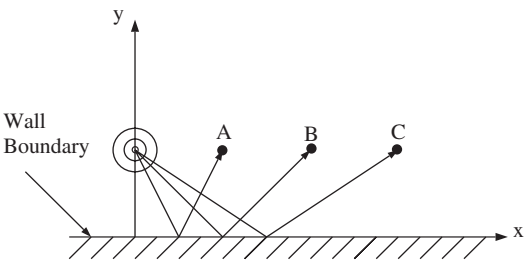

Figure 8. Explanation of initial value problem for comparison of leapfrog type schemes.

second-order upwind leapfrog method is more than that of Yee's scheme but its accuracy is higher than Yee's schemes. Therefore, the efficiency of both schemes are comparable. To confirm that comparison, a simple initial value problem is devised as shown in Figure 8. Initial values are

$$p(x, y) = \exp\left(-\frac{\ln 2}{5^2}[x^2 + (y - 20)^2]\right)$$

$$u(x, y) = v(x, y) = 0$$

The positions of the points A, B and C are (20,20), (40,20) and (60,20). Ghost cells are generated with mirror images for wall boundary treatment. The courant numbers (v_x, v_y) are $\frac{1}{4}$. Pressure values are measured at each point and compared on various grid sizes. Measuring times of the points A, B and C are 45, 50 and 70. Figure 9 presents the grid convergence histories of each point. The results of the second-order schemes (Figure 9(a), (c), (e)) show very similar accuracy level. However, the fourth-order results (Figure 9(b), (d), (e)) demonstrate distinct deviations between two results. The fourth-order upwind leapfrog scheme updates accurate solutions with even coarse grid.

3. UPWIND LEAPFROG METHODS IN POLAR CO-ORDINATES

In polar co-ordinate (r, θ, t) with velocity components, u and v, the acoustic equations in dimensionless form are

$$\begin{aligned} \frac{\partial p}{\partial t} + \frac{\partial u}{\partial r} + \frac{1}{r}\frac{\partial v}{\partial \theta} + \frac{u}{r} &= 0 \\ \frac{\partial u}{\partial t} + \frac{\partial p}{\partial r} &= 0 \\ \frac{\partial v}{\partial t} + \frac{1}{r}\frac{\partial p}{\partial \theta} &= 0 \end{aligned} \tag{26}$$

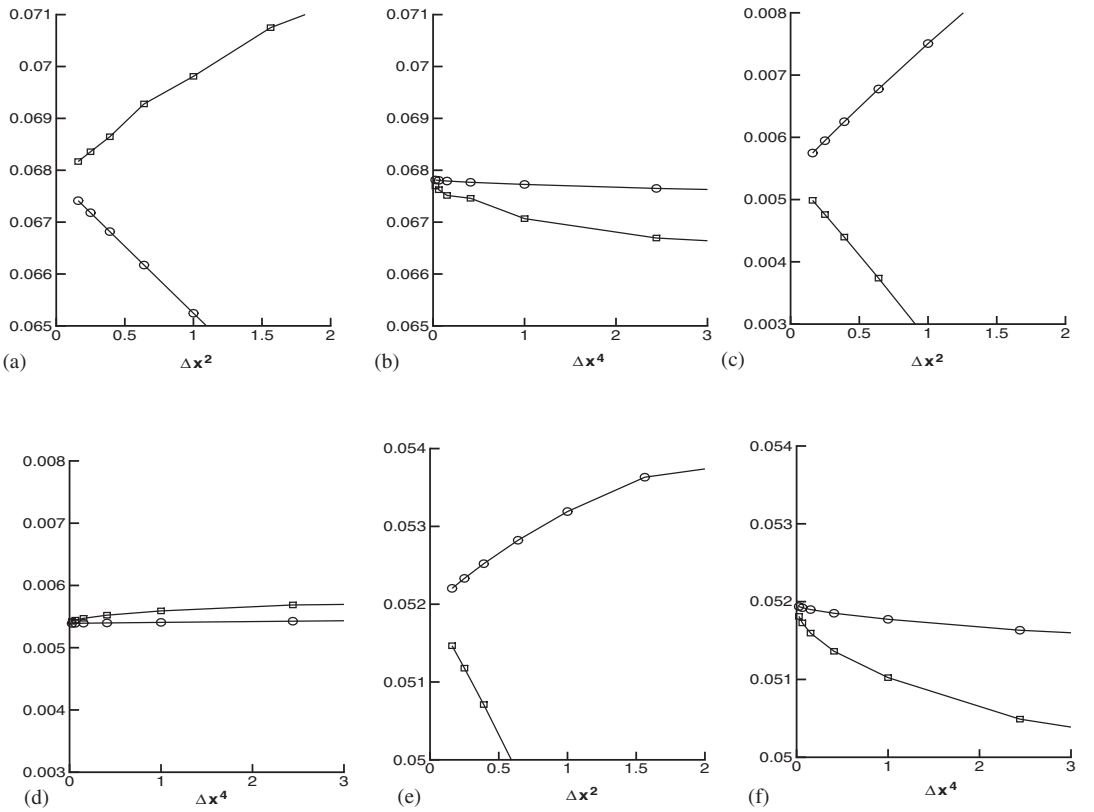

Figure 9. Grid convergence histories, circle: upwind leapfrog, square: Yee's standard leapfrog method: (a) Point A, $t=45$ order, second order; (b) Point A, $t=45$ fourth order; (c) Point B, $t=45$ second order; (d) Point A, $t=45$ fourth order; (e) Point C, $t=45$ second order; and (f) Point A, $t=45$ fourth order.

Bicharacteristic version of these equations, aligned respectively along radial and circumferential directions, are

$$\frac{\partial}{\partial t}(p \pm u) \pm \frac{\partial}{\partial r}(p \pm u) + \frac{1}{r}\frac{\partial v}{\partial \theta} = -\frac{u}{r} \tag{27}$$

$$\frac{\partial}{\partial t}(q \pm v) \pm \frac{1}{r}\frac{\partial}{\partial \theta}(q \pm v) + \frac{\partial u}{\partial r} = -\frac{u}{r} \tag{28}$$

Compared with their Cartesian counterparts, these equations have source terms on the right-hand side, which require special techniques to avoid exciting long-term instabilities. Those techniques are described in Reference [9] in detail and omitted here. However, the source term of Equation (28) is independent of the updated variables $(q \pm v)$ and was discretized time-reversibly by replacing the term, u/r with $(u^n_{j-1/2,k} + u_{j+1/2,k})/2r_{j,k}$.

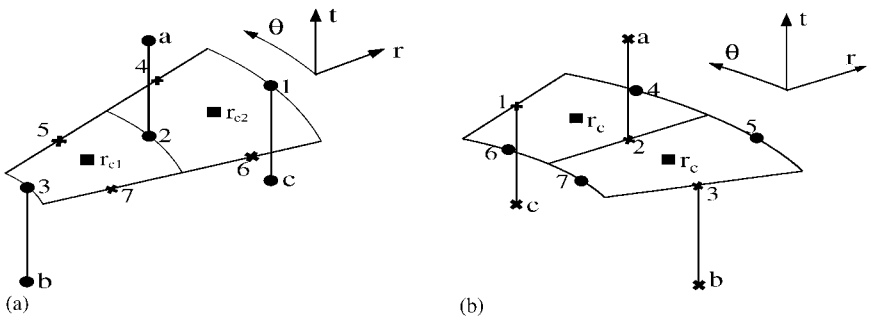

Figure 10. Second-order stencils for acoustics in polar co-ordinate: (a) $(p \pm u)$ waves; and (b) $(q \pm v)$ waves.

For stable discretization, however, Equation (27) were transformed to Equations (29)

$$\frac{\partial}{\partial t}\left(p \pm \frac{r}{r_c}u\right) \pm \frac{\partial}{\partial r}\left(p \pm \frac{r}{r_c}u\right) + \frac{1}{r}\frac{\partial v}{\partial \theta} = 0 \tag{29}$$

and the second-order discretizations based on the stencil, Figure 10(a) are

$$\begin{aligned} &\delta_t\left(p + \frac{r}{r_j}u\right)^{n+1/2}_{j+1/2,k} + \delta_t\left(p + \frac{r}{r_j}u\right)^{n-1/2}_{j-1/2,k} + 2v_r\delta_r\left(p + \frac{r}{r_j}u\right)^{n}_{j,k} + 2v_\theta\delta_\theta v^n_{j,k} = 0 \\ &\delta_t\left(p - \frac{r}{r_j}u\right)^{n+1/2}_{j-1/2,k} + \delta_t\left(p - \frac{r}{r_j}u\right)^{n-1/2}_{j+1/2,k} - 2v_r\delta_r\left(p - \frac{r}{r_j}u\right)^{n}_{j,k} + 2v_\theta\delta_\theta v^n_{j,k} = 0 \end{aligned} \tag{30}$$

where $v_r = \Delta t/\Delta r$ and $v_\theta = \Delta t/(r\Delta\theta)$. This stabilizing technique was also applied to the fourth-order schemes in a similar way.

4. NUMERICAL EXPERIMENTS

The second- and fourth-order upwind leapfrog schemes developed in the previous sections were applied to typical acoustic problems such as the piston problem and the acoustic scattering from a cylinder to evaluate their applicability to real acoustic simulation.

4.1. Piston problem simulation

The acoustic wave produced by an oscillating piston with an axisymmetric infinite baffle (Figure 11) was simulated to test the numerical scheme. This problem is governed by the linearized axisymmetric Euler equations whose characteristic form is

$$\frac{\partial}{\partial t}(p \pm u) \pm \frac{\partial}{\partial x}(p \pm u) + \frac{\partial v}{\partial y} = -\frac{v}{y} \tag{31}$$

$$\frac{\partial}{\partial t}(p \pm v) \pm \frac{\partial}{\partial x}(p \pm v) + \frac{\partial u}{\partial x} = -\frac{v}{y} \tag{32}$$

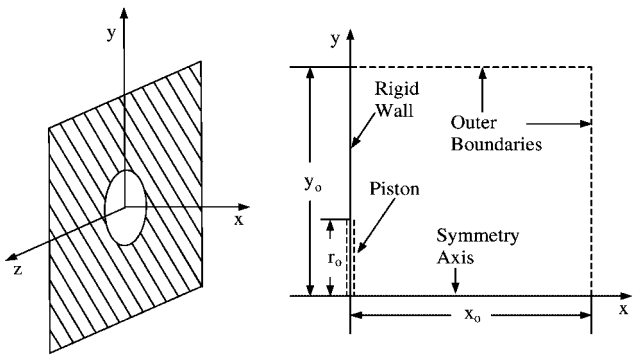

Figure 11. Geometry of axisymmetric piston problem.

The analytic solution for the magnitude of the pressure oscillations along the axis of symmetry [10] is given as

$$\frac{P(x)}{2\rho_0 a_0 U} = \left| \sin\left(\frac{\pi f x}{a_0} \left[\sqrt{1 + \left(\frac{r_0^2}{x} \right)^2} - 1 \right] \right) \right| \tag{33}$$

where P is the magnitude of pressure oscillation, U is the piston displacement magnitude, f is its frequency and r_0 is its radius. Equation (33) shows that the axial pressure magnitude is function of f, r_0 and x for given ρ_0, a_0 and U. For simplicity ρ_0, a_0 and U are set to one. The axisymmetric equations also have a source term, $-v/y$ which is independent of $(p \pm u)$ and it was discretized by central differencing. However, the source term of Equation (32) is dependent on $(q \pm v)$ and it requires a stabilizing technique described in Section 4. Three-level second-order upwind leapfrog schemes were implemented for this experiment. The frequency f is chosen as ten cycles per unit time and r_0 equal to $\frac{1}{10}$ of unit length. The computational domain is $0 \leqslant x \leqslant 1.0$ and $0 \leqslant y \leqslant 1.0$. Figure 12 shows the contour plot of acoustic field. The grid size used for this computation and the Courant number were 120×120 and $\frac{1}{2}$, respectively. Most of the acoustic energy was transmitted along the axis of symmetry and a smaller portion was radiated diagonally. Giles' second-order boundary condition was implemented at the far-field and little outgoing acoustic wave was reflected. Pressure magnitudes along the axis were compared with the analytic solution for various grid size in Figure 13 and the results exhibit good agreement with the analytic solution even on the coarse grid (8 cells per wavelength). As the grid is refined, the numerical results converged to the analytic solution.

4.2. Acoustic scattering from a cylinder

One of the second computational aeroacoustics benchmark problems [11] was simulated to test the fourth-order upwind leapfrog scheme in cylindrical coordinates. Pressure pulse initially distributed in Gaussian propagates outside as time goes on and reflected from a circular

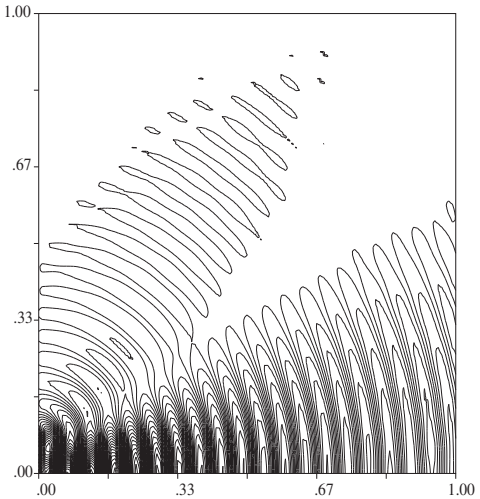

Figure 12. Pressure contour plot of piston problem. $\Delta x = \Delta y = \frac{1}{12},\ t = 3.0$.

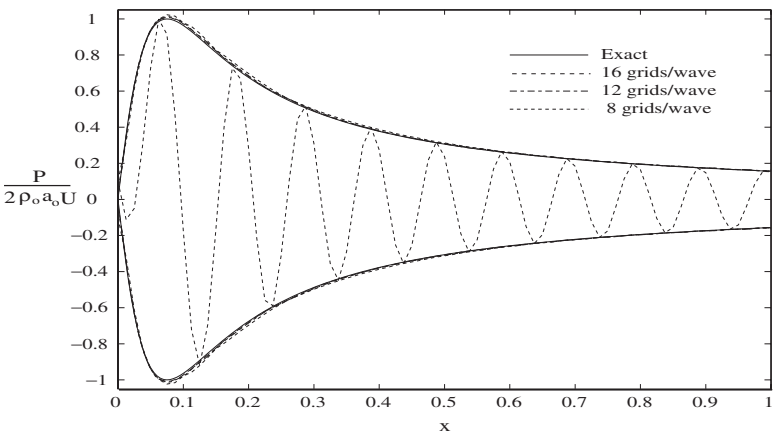

Figure 13. Comparison of numerical pressure envelopes with analytic solution for various grid sizes.

cylinder. This example is explained in Figure 14 and the governing equations are

$$\begin{aligned} \frac{\partial p}{\partial t} + \frac{\partial u}{\partial r} + \frac{1}{r}\frac{\partial v}{\partial \theta} + \frac{u}{r} &= 0 \\ \frac{\partial u}{\partial t} + \frac{\partial p}{\partial r} &= 0 \\ \frac{\partial v}{\partial t} + \frac{1}{r}\frac{\partial p}{\partial \theta} &= 0 \end{aligned} \tag{34}$$

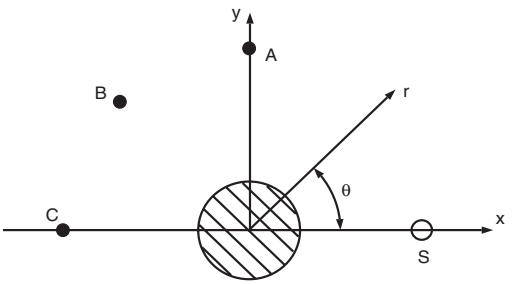

Figure 14. Geometry of acoustic scattering problems.

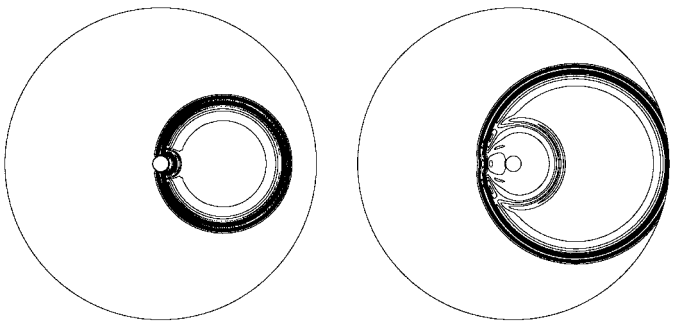

Figure 15. Pressure pulse contours of initial value problem simulation. $0.5 \leqslant r \leqslant 10.0$, $\Delta r = 1/14$.

where u and v are the disturbed velocities in radial and azimuthal directions. Ghost cell values are generated around the cylinder for the wall boundary condition and Thompson's characteristic boundary condition [12] was implemented at the far-field boundary. The given initial values are

$$p(x, y) = \exp\left(-\frac{\ln 2}{0.2^2}[(x-4)^2 + y^2]\right)$$
$$u(x, y) = 0, \quad v(x, y) = 0 \tag{35}$$

As time goes on, pressure pulse propagates outward and is reflected from the cylinder wall. Pressure value was measured at three chosen points $A(r = 5, \theta = 90^\circ)$, $B(r = 5, \theta = 135^\circ)$, $C(r = 5, \theta = 180^\circ)$. Measuring time was from $t = 6$ to $t = 10$. Measured pressure values were compared to analytic ones. Figure 15 presents contour plots of the results at $t = 4.0$ and 6.0, according to the fourth-order scheme with $\Delta r = \frac{1}{14}$. When $t = 4.0$, the wave front is reflected from the cylinder while most of the pressure pulse propagates outside. At later time ($t = 6.0$) the reflected wave follows the main pulse and there is a continuous front around the cylinder. Time histories of pressure at points (A, B and C) are shown in Figure 16.

The second-order results were presented by the solid line for various grid sizes ($\Delta r = \frac{1}{24}, \frac{1}{32}, \frac{1}{40}$) and the analytic solution was expressed by the dotted line in Figure 16(a). The numerical

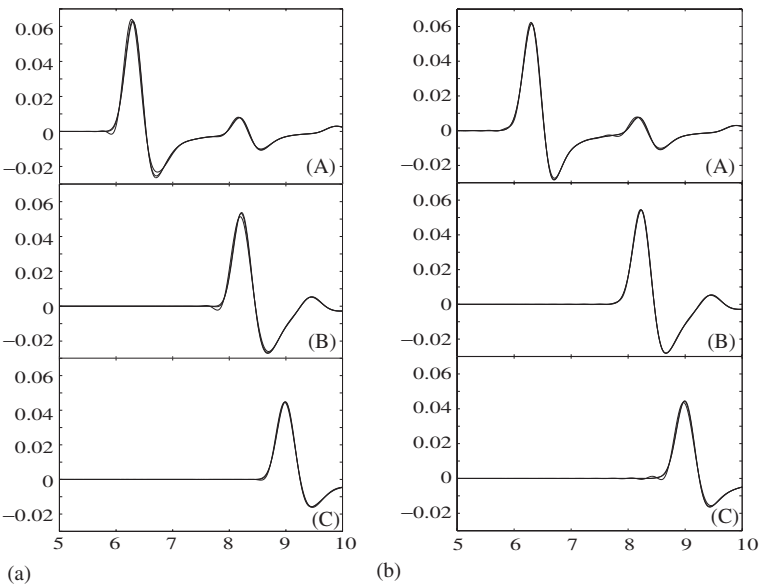

Figure 16. Pressure histories of (a) second- and (b) fourth-order scheme at point A(top), B(middle) and C(bottom). Dotted line: analytic solution. $5 \leqslant t \leqslant 10$, $\Delta r = \frac{1}{24}, \frac{1}{32}$ and $\frac{1}{40}$.

result indicated some deviation from the analytic solution even on the finest grid ($\Delta r = \frac{1}{40}$). On the other hand, Figure 16(b) presents the fourth-order results on grids with ($\Delta r = \frac{1}{12}, \frac{1}{16}, \frac{1}{20}$). The numerical solution on the coarsest grid ($\Delta r = \frac{1}{12}$) produced notable oscillations at point A and C, but the numerical result with $\Delta r = \frac{1}{16}$ demonstrated good agreement with the analytic solution. In order to confirm that these results do in fact have the formal accuracy, the pressure at one particular place and time was plotted against the second or fourth power of the mesh size. Such a plot should yield a straight line which intecepts at $\Delta r = 0$ and it is considered a deferred approach to the limit, the best numerical estimate of the analytic solution. The first pressure minima ($t = 6.7$) measured at point A are plotted in Figure 17 against Δr^2. The star (*) on the vertical axis represents the analytic solutions although numerical solution converges to a value not far from the analytic solution.

The fourth-order results are plotted in Figure 17(b) against Δr^4 in the range, $1/\Delta r = 14-30$. As indicated from the Fourier analysis, the errors are much lower and a grid-converged solution is very close to the analytic one. To examine how well the wall boundary condition works, the second pressure minimum values ($t = 8.6$) are measured at point A and plotted in Figure 18. Results indicated again that the fourth-order methods are more accurate and convincing.

They seem to be headed rather precisely for the analytic solution, and the minute discrepancy might be due to small errors in the wall boundary condition. It is conceded that neither the starting procedure nor the surface boundary condition is beyond reproach, but their effect appeared to be so small numerically that the code behaved for all practical purposes as if it were fourth-order accurate.

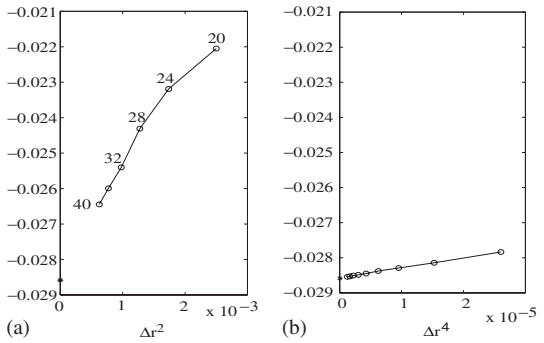

Figure 17. Grid convergence studies for the pressure of Point A at the first pressure minimum: (a) second-order; and (b) fourth-order. *: Analytic solution.

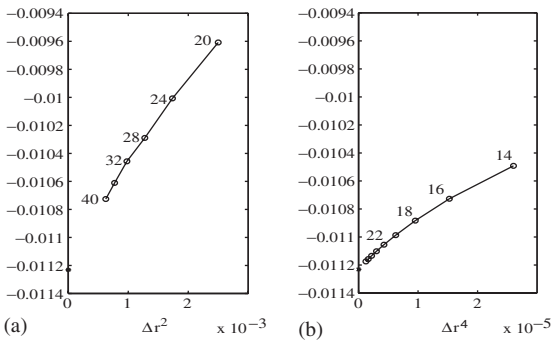

Figure 18. Grid convergence studies for the pressure of Point A at the second pressure minimum: (a) second-order; and (b) fourth-order. *: Analytic solution.

5. CONCLUSION

One-dimensional version of the upwind leapfrog method was successfully extended to multi-dimensional acoustics. The stability limitation of two-dimensional higher-order scheme was overcome and it is stable even on non-square grid as well as for the system of equations having source term proportional to the solution. Furthermore, numerical experiment results of several test cases also assure the accuracy of the upwind leapfrog scheme. Since the stencil of the higher-order scheme, however lies over one grid cell, further investigation on the computational boundary treatment is needed if a higher-order accuracy is to be maintained.

ACKNOWLEDGEMENTS

I would like to express my deep appreciation to Professor P. L. Roe for his insight and thoughtful discussion on this research.

REFERENCES

1. Zingg DW. A Review of High-Order and Optimized Finite-Difference Methods for Simulating Linear Wave Phenomena. AIAA Paper 97-2088, *13th AIAA Computational Fluid Dynamics Conference*, Snowmass, June, 1997.
2. Iserles A. Generalised leapfrog methods. *IMA Journal of Numerical Analysis* 1986; **6**.
3. Roe PL. Linear bicharacteristic schemes without dissipation. *SIAM Journal of Scientific Computing* **19**(5).
4. Thomas JP, Roe PL. Development of non-dissipative numerical schemes for computational aeroacoustics. AIAA Paper 93-3382, In *AIAA 11th Computational Fluid Dynamics Conference*, 1993.
5. Thomas JP, Kim C, Roe PL. Progress towards a new computational scheme for aeroacoustics. AIAA Paper 95-1758, In *AIAA 12th Computational Fluid Dynamics Conference*, 1995.
6. Nguyen BT. Investigation of three-level finite difference time-domain methods for multidimensional Acoustics and electromagnetics. *Ph.D. Thesis*, Department of Aerospace Engineering, University of Michigan, 1996.
7. Kim C. Accurate multi-level schemes for advection. *International Journal for Numerical Methods in Fluids* 2003; **41**:471–494.
8. Thomas JP. An investigation of the upwind leapfrog method for scalar advection and Acoustic/aeroacousticwave propagation problems. *Ph.D. Thesis*, Department of Aerospace Engineering, University of Michigan, 1996.
9. Kim C. Maintaining the stability of a leapfrog scheme in the presence of source terms. *International Journal for Numerical Methods in Fluids* 2003; **42**:839–852.
10. Kinsler LC, Frey AR, Coppens AB, Sanders JV. *Fundamentals of Acoustics*. Wiley: New York, 1982.
11. Tam CKW, Hardin JC (ed). *Second Computational Aeroacoustics* (*CAA*) *Workshop on Benchmark Problems*, NASA Conference Paper 3352, June, 1997.
12. Thompson KW. Time dependent boundary conditions for hyperbolic systems. *Journal of Computational Physics* 1987; **68**:1–24.

